Hindawi
Geofluids
Volume 2023, Article ID 5173170, 19 pages
https://doi.org/10.1155/2023/5173170

Research Article

An Experimental Study with Model Calibration for the Permanent Strain of Granite Residual Soil Subgrade under Drying-Wetting Cycles

Xuefei Yang[1], **Dongxia Chen**[1], **Yue Liu**[1] and **Sheng Zhang**[2]

[1]*Department of Civil Engineering, Fujian Key Laboratory of Digital Simulations for Coastal Civil Engineering, Xiamen University, Xiamen 361005, China*
[2]*National Engineering Laboratory for High-Speed Railway Construction Technology, Changsha 410075, China*

Correspondence should be addressed to Dongxia Chen; dongxiachen@xmu.edu.cn and Sheng Zhang; zhsh1230@126.com

Received 30 August 2022; Revised 10 October 2022; Accepted 13 October 2022; Published 4 February 2023

Academic Editor: Dongjiang Pan

The permanent strain is one of the most important dynamic properties of the granite residual soil. To systematically study the dynamic deformation characteristics of granite residual soil (GRS) under the drying-wetting (D-W) cycles, a series of dynamic triaxial tests is carried out to obtain the stress-strain relationship of GRS with various fine particle contents subjected to D-W cycles. The experimental results show that the growth of permanent strain consists of two stages, namely, compaction stage and compression stage. The main effect of D-W cycles is reflected in the compression stage. On the other hand, the influence of fine particle contents on the permanent strain occurs mainly at the compaction stage, which can be classified as the lubrication, densification, and asphyxiation, respectively. Subsequently, a new criterion to characterize the permanent strain of GRS is deduced from the experimental results, which accounts for both strains and rates of strains. This criterion illustrates that with the increase of D-W cycles number, the permanent strain evaluation pattern of GRS is gradually changing from plastic stabilization to plastic creep. Finally, a quadratic function model referring to the log-log scale is proposed to fit well the relationship between the permanent strain and loading cycle number of GRS under D-W cycles. It is found that the parameters of the proposed model can physically represent the strain rate, the compression strain, and the compaction strain.

1. Introduction

Granite residual soil (GRS) is generally found in many tropical regions [1], especially in southern China. In engineering practice, it is inevitable to use in-place GRS as filling materials in the construction of expressway or high-speed railway in these areas. GRS exhibits certain unfavorable characteristics, such as high mica content, loose structure, water sensitivity, and low cohesion [2–5]. Under drying condition, GRS has relatively high shear strength and low compression properties, which can meet the requirements of most project constructions [6, 7]. However, in case of wetting condition, it is found that an interlayer between coarse and fine particles can be easily formed in some railway or highway subgrades which are filled with GRS under dynamic loading [8, 9]. This is because that the geotechnical properties of GRS will significantly deteriorate with an increase in water content [10, 11]. This interlayer affects the shear strength and compression properties and leads to serious roadbed problems, i.e., uneven subgrade settlement, track irregularity, and subgrade mud pumping [12]. Furthermore, the GRS subgrades are usually subjected to seasonal drying and wetting cycles (D-W cycles) for subtropical monsoon climate [5, 13], and the intergranular soil bonds become fragile and cause typical fatigue damages such as reduced clay particles, coarsened pores, and loose structure [14].

In the meantime, due to the train vibration, the slip and dislocation among particles often crush the coarse particles, and the reciprocating migration of the pore water drives the movement of the internal fine particles [15, 16]. All of these not only lead to further propagation of existing weathering

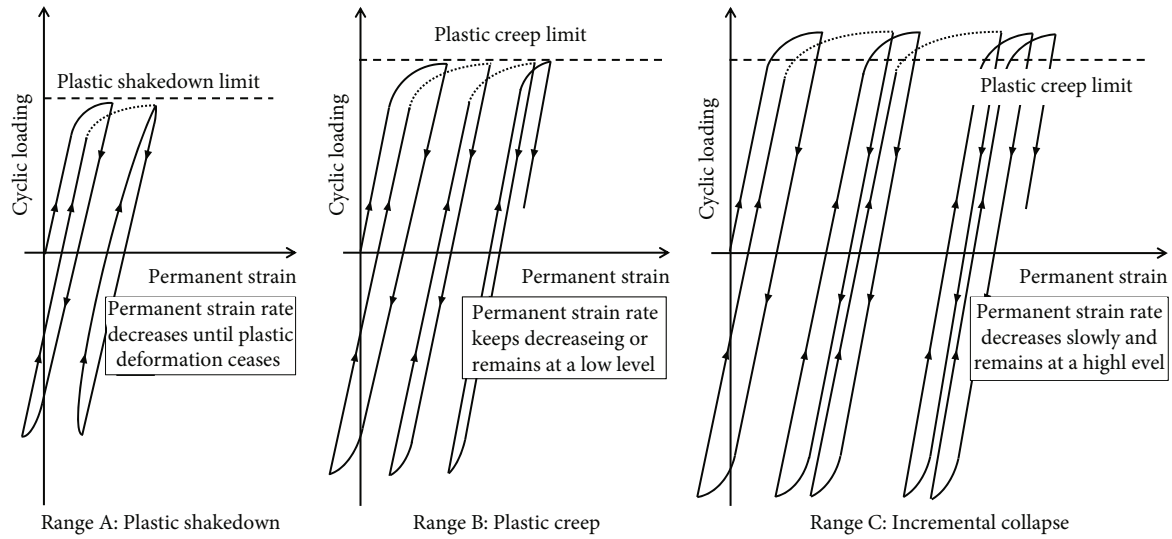

Figure 1: A schematic diagram of characterizing the shakedown ranges of the permanent strain development of a granular material under cyclic loading.

Table 1: The physical parameters of soil.

Group	Increased fine particle content ($d < 0.075$ mm)/%	Plastic limit PL/%	Liquid limit LL/%	Optimal water content w_{op}/%	Maximum dry density ρ_{dmax} /g cm^{-3}
K0	0	23	47	20.3	1.65
K10	10	30	52	21.6	1.68
K20	20	28	44	22.0	1.67
K30	30	24	47	23.3	1.65

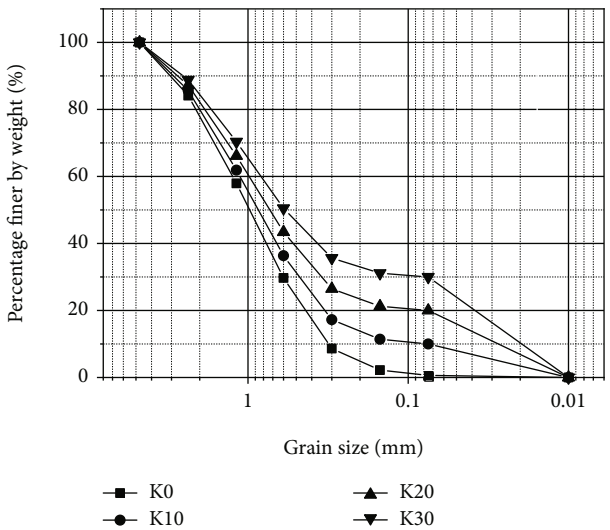

Figure 2: Particle size distribution curves.

cracks and accelerate the formation of coarse-fine grain interlayers of GRS, but also yield irreversible structural damage and fatigue failure of subgrades. Therefore, it is essential to study the effects of D-W cycles on the dynamic characteristics of GRS.

Figure 3: Soil samples.

It has been widely accepted that the permanent strain $\Delta\varepsilon_{ap}$ is a significant characteristic of the dynamic properties of soils [17]. The permanent strain has been investigated under various influencing factors, such as confining pressure, consolidation ratio, loading amplitude, and vibration frequency, through dynamic triaxial tests [18–21]. The $\Delta\varepsilon_{ap}$ of GRS under dynamic loading is a gradual process. The shakedown theory has been commonly adopted to characterize this process under cyclic loading. This theory classifies the deformation behaviors into three groups (Range A: plastic shakedown, Range B: plastic creep, and Range C: incremental collapse), as shown in Figure 1. In the subgrade design, the subgrade must be able to resist permanent deformation. To ensure that a subgrade has desirable rutting resistance, the design guide suggests selecting the base materials from Range A and Range B and avoids using the base materials from Range C [22]. The base materials from Range C should be strictly avoided in practice because of the severe settlement or even failure of the superstructure caused by permanent strain, such as the rutting or cracking at the pavement surface and the differential settlement of track systems. To define the shakedown boundaries, Werkmeister et al. [22] divided three groups by the difference between the permanent axial strains corresponding to 5000 and 3000 loading cycles

(a) Constant temperature oven (b) Spray humidify

Figure 4: The drying process and wetting process.

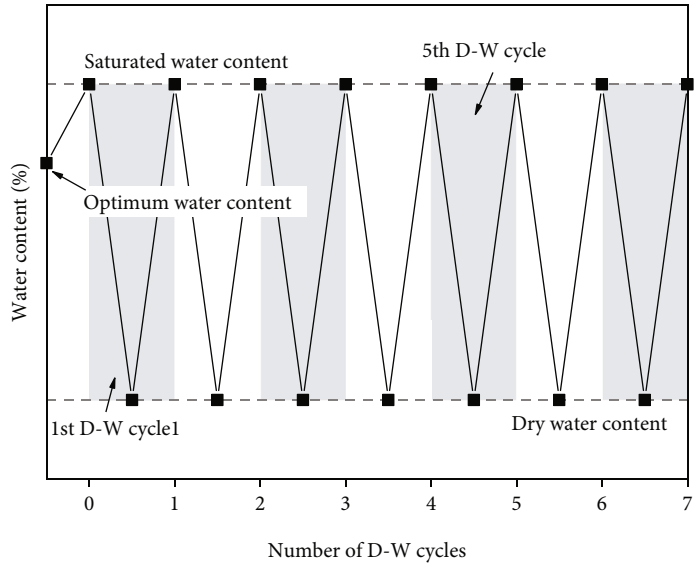

Figure 5: D-W cycle paths of soil samples.

($\Delta\varepsilon_{ap,5000} - \Delta\varepsilon_{ap,3000}$). However, these criteria based only on 3000th to 5000th cycles, for some kinds of base materials, the postcompaction compression may not be completed by the end of the 5000th cycle. To address this limitation, Chen et al. [18] proposed the criteria to characterize the shakedown range by the development rate of plastic strain in the second stage. But these criteria are developed merely based on a limited number of cyclic loading triaxial test. Whether these criteria are suitable for other base materials is still unknown. Thus, these criteria should be reevaluated for local base materials such as GRS.

Many investigations on the dynamic behaviors of base materials had been conducted, and various models have been developed to determine the relationship between the accumulated permanent strain and the number of cyclic dynamic loading. To quantify the influence of load conditions on the strain characteristics of GRS, Li et al. used an improved power function to fit the relationship between permanent strain and load times which enhanced the model's correlation at small load times [23]. Yin et al. employed the strain model of soft clay to describe the permanent strain of the GRS under different water content and confining pressure and analyzed the relationship between fitting parameters and confining pressure, load amplitude, water content, and other variables [8]. Tang et al. proposed a nonlinear creep model of GRS, which considers the accumulation of residual stress under the dynamic loading of subgrade combined with rheological theory and the creep behavior of GRS [24]. This model can better predict the creep characteristics of GRS under cyclic dynamic loading, but it is not well applied to more complicated situations, such as D-W cycles. These prediction models do not take into account the fine particle contents of subgrade subjected to D-W cycles. However, the existing studies demonstrated that these factors significantly affect the permanent deformation behavior of GRS [18, 20]. Thus, new prediction models should be developed for GRS in a manner that permanent deformation properties are correlated to D-W cycles and fine particle contents of GRS.

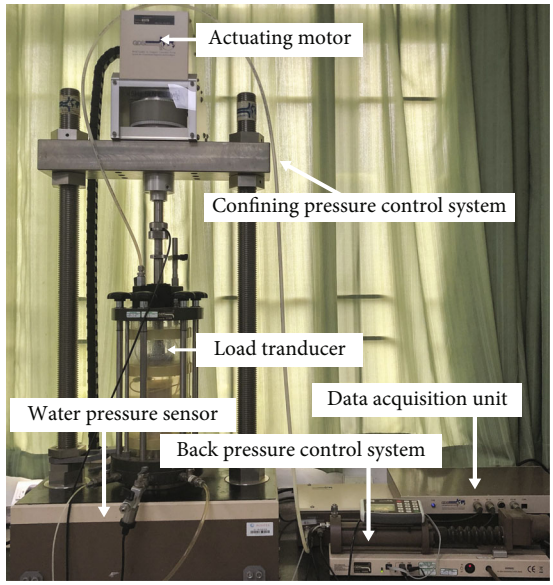

Figure 6: GDS standard dynamic triaxial test system.

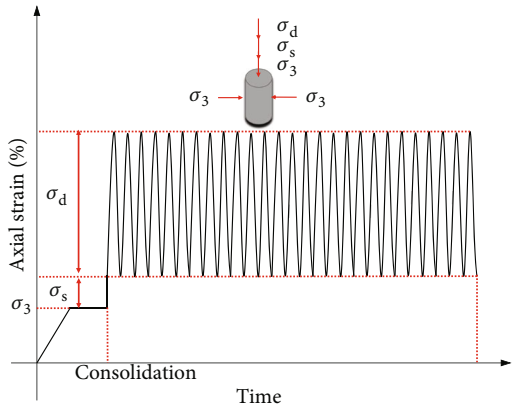

Figure 7: Load diagram.

In terms of the influence of D-W cycles on the soil property, Kong et al. [3] used NMR technology and found that the water-holding capacity of soil decreases with the increase of D-W cycles, which is the most obvious in the first D-W cycles and tended to be stable after the fourth D-W cycles. Liu et al. [4] performed triaxial shear tests on GRS after D-W cycles and found that the dilatancy effect of GRS after D-W cycles is greater than that without D-W cycles, and the dilatancy effect reduces with the increase in the number of D-W cycles. To quantify the damage law of GRS after D-W cycles, An et al. [14] used the resistivity stress-strain model to effectively predict the stress-strain curve of soil after D-W cycles by introducing the initial damage factor. Nonetheless, the effect mechanism of D-W cycles on soil microstructure needs to be studied. However, there is no unified understanding of the discussion on the microstructure change of GRS under D-W cycles in current, and the change of microstructure cannot explain the macroscopic characteristic mechanism.

The above works mainly concentrate on the permanent strain of soil based on dynamic triaxial tests. In the meantime, it is noted that the particularity of mineral composition and grain composition leads to the complex permanent strain of GRS, but few studies in the open literatures describe in detail the dynamic properties of GRS, especially the permanent strain, and explain the dynamic mechanism of GRS under the D-W cycles. Consequently, the evaluation of the engineering characteristics of GRS is usually over conservative. Therefore, this work focuses on the analysis of the permanent strain of GRS under the influence of D-W cycles and fine particle contents. Through dynamic triaxial tests under cyclic loading, this work presented a detailed study on the effects of D-W cycles and fine contents on permanent strain of GRS in Fujian, China. Based upon the existing shakedown theories, a new criterion was proposed to clarify different deformation types. The influence mechanism of D-W cycles and fine particle contents on the permanent strain of GRS was analyzed by combining the new criterion and soil microstructure. Finally, a fitting model was established to predict $\Delta\varepsilon_{ap}$ of GRS subjected to D-W cycles.

2. Experimental Setup

Four fine particle contents, seven D-W cycles, and other test conditions are considered in this study to examine the permanent strain of GRS and the effects of D-W cycles.

2.1. Preparation of Materials. The tested GRS was collected from the edge of a railway subgrade in Xiamen, Fujian Province, China. The sampling site has hilly landforms in the GRS area with a depth of 2 m~4 m. In order to meet the requirements of high-speed railway base bed fillers in accordance with the Code for Design of Railway Earth Structure (TB10001-2016) [25], the fine particle contents were selected as 0%, 10%, 20%, and 30%, and the influence of fine particle contents on the deformation characteristics of GRS after D-W cycles was then analyzed.

The optimal water content and maximum dry density were obtained from the compaction test curves of different fine particle contents. The basic physical properties of the adjusted soil samples are measured and listed in Table 1. The particle size distributions of soil samples after adjustment are plotted in Figure 2. All soil samples were configured according to the optimal water content of each group.

The soil was placed in a split mold with an internal height of 100 mm and a diameter of 50 mm. Static compaction was performed in five equal layers to obtain a dry density of 95% of the optimum Proctor normal ρ_{dmax}. The weight and height of each layer were measured, which allowed to obtain a homogeneous density, and only those below a 1% error were tested. The prepared soil samples were immediately wrapped with plastic wrap to prevent moisture from evaporating, as shown in Figure 3.

2.2. D-W Cycles for Soil Samples. To simulate the real railway subgrade site conditions and the natural environmental changes experienced after construction, the soil samples were prepared through the following steps:

Table 2: Cyclic triaxial test conditions.

Group	Cycle path w/%	D-W cycle number n	Confining pressure σ_3 /kPa	Amplitude σ_d /kPa	Load frequency f /Hz
K0/K10/K20/ K30	Saturated-10-saturated (55°C)	0~7	60	60	2

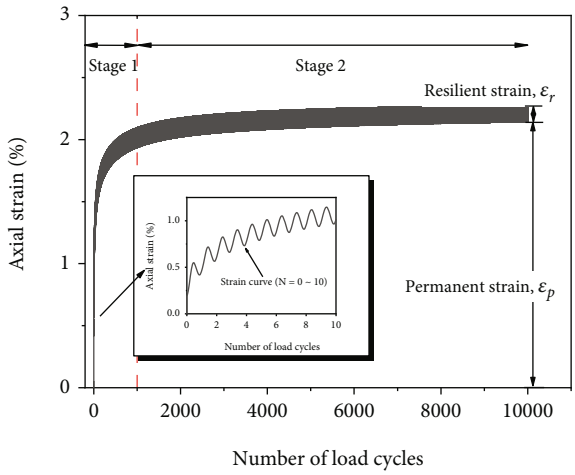

Figure 8: Strain curve of GRS under train vibration excitation.

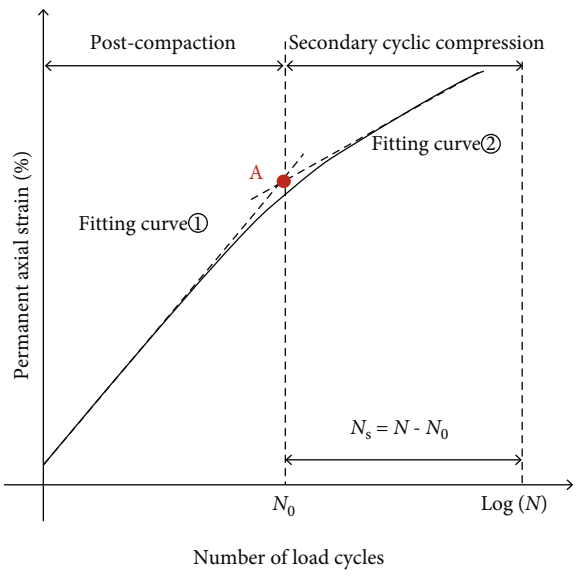

Figure 9: Determination of critical load times.

(1) *Preparing Saturation Samples*. All samples with optimum water content should be wetted to saturate first. The sample wetted from optimum water content to saturated water content for the first time is 0 D-W cycle

(2) *Drying Process*. The samples were dried for 6 hours continuously by a constant temperature oven at a temperature of 55°C (the highest soil surface temperature in summer in Xiamen, Figure 4). The mass of the soil sample was measured each hour to ensure the moisture evenly evaporated during the drying process. By parallel measurements, the water content of the soil samples after drying basically keeps around 10.0%

(3) *Wetting Process*. The spray humidifying method was used during the sample wetting process: pasted the wet filter papers around the sample (Figure 4), and then sprayed water evenly and intermittently (one spray every 10 minutes) by an electric spray device. Subsequently, the soil sample mass was continuously monitored during the wetting process, until the mass reached a constant and the water content no longer changed. Thus, one D-W cycle of the soil sample was completed

(4) Repeating the second and third steps, while the number of replications was based on the number of cycles required. The D-W cycles paths are illustrated in Figure 5. Thus, samples under different numbers of D-W cycles were prepared completely

(5) *Saturation Process*. Considering the most unfavorable situation of subgrade water damage, the triaxial test was performed for the soil samples under saturated conditions. The saturation process was divided into two steps: vacuum saturation and back-pressure saturation. First, vacuumed samples by a vacuum pump for 2 hours, and then closed the vacuum pump valve and filled the water level to 3/4 of the soil sample height. Second, opened the vacuum pump for another 2 hours, and kept samples under 1 standard atmosphere pressure for 24 hours. Back-pressure saturation was used to install the soil sample in a dynamic triaxial instrument by applying back pressure to monitor the pore water pressure coefficient B, and when the value of B reached above 95%, the saturation process ended

2.3. Dynamic Triaxial Tests. As shown in Figure 6, the British GDS standard dynamic triaxial test system was used. The apparatus consists of actuating motor, confining pressure control system, back-pressure control system, and data acquisition unit. The allowable maximum dynamic load frequency and axial force are 5 Hz and 5 kN, respectively.

Generally, the action time of the train load is relatively short so that the subgrade water is not easy to drain, and thus the subgrade must bear both the cyclic dynamic load by moving trains and the static deviation stress by

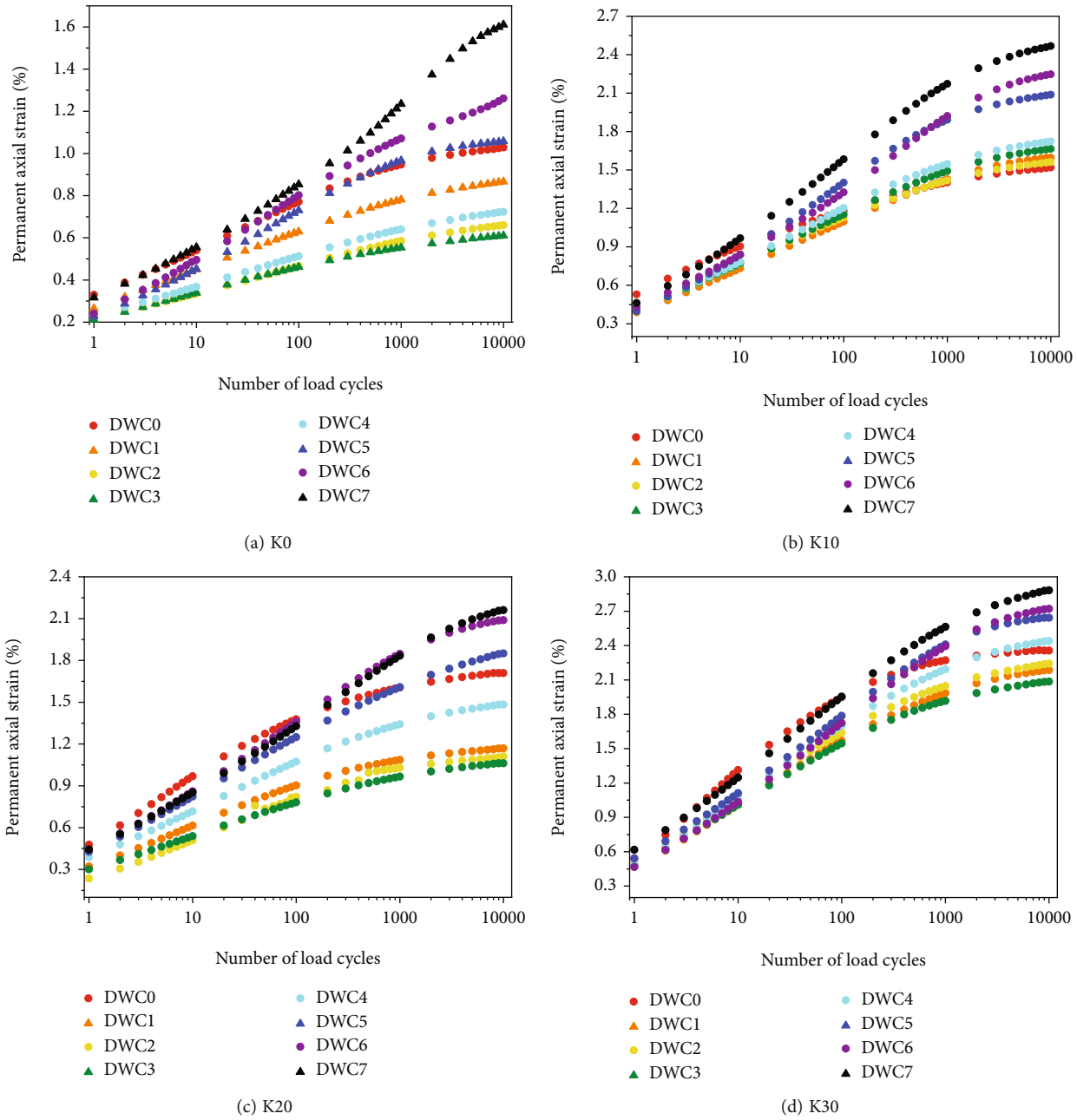

Figure 10: Permanent axial strain of GRS under D-W cycles.

superstructures, such as the overlying soil and sleeper and rail. Therefore, this experiment was subjected to a partial sine wave dynamic load under undrained conditions as shown in Figure 7. The saturated soil sample was consolidated isotropically, a static load σ_s of 15 kPa was applied to simulate the action of the superstructure, and then the dynamic stress with the same amplitude was added to simulate the dynamic train load. Given the influence of D-W cycles and the limited depth of train load (1-5 m below the surface), the consolidation confining pressure σ_3 of 60 kPa was chosen.

Normally, the dynamic load of high-speed railway trains is between 30 kPa and 70 kPa, so the dynamic load amplitude σ_d of 60 kPa was adopted [26]. The loading frequency lied between 1 and 5 Hz according to the speed of high-speed railway. Therefore, the loading frequency of dynamic load was set as 2 Hz. During the loading process, when the axial strain of the sample exceeded 10%, it was considered that the deformation of the sample was too large which would result in the soil sample failure. Meanwhile, when the permanent strain tended to be stable and the vibration times reached 10,000, the experiment was terminated [27]. The testing scheme in this study was explained in Table 2.

3. Testing Results

The permanent strain presents an upward convex and stable development trend when the GRS is subjected to dynamic

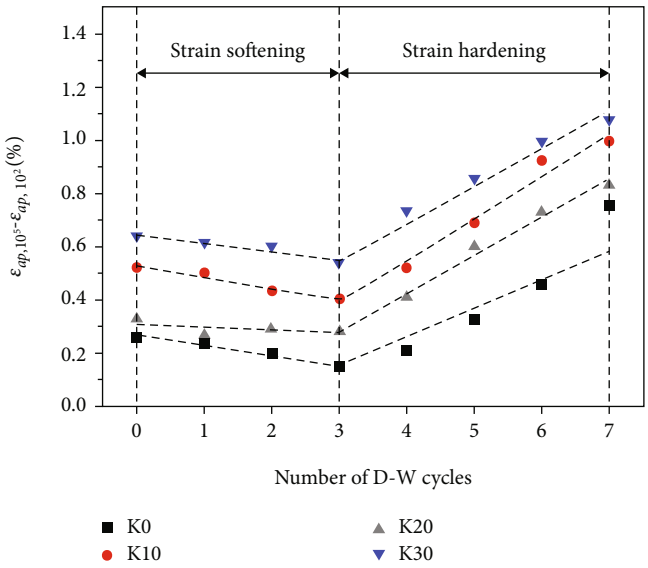

FIGURE 11: Relationship between permanent strain of GRS and number of D-W cycles in the compression stage.

loads, as shown in Figure 8. The development of $\Delta\varepsilon_{ap}$ comprises two parts: the postcompaction stage and the secondary cyclic compression stage. The postcompaction stage is a conditioning period during which initial particle breakage, particle rearrangement, and unrecoverable interparticle slip happen [28, 29]. The centers of particles are compressed closer, and the areas of interparticle contacts become larger to stabilize the granular material to adapt to the current applied loading [30, 31]. During the secondary cyclic compression period, there is progressive development of $\Delta\varepsilon_{ap}$, mainly along with interparticle slip and limited particle attrition or breakage [17]. The postcompaction stage is only experienced once in the field, and the strain development trend in this period is arbitrary. The secondary cyclic compression stage is the condition that a granular material layer actually exhibits in the field. The criterion to distinguish these two parts is the sudden change in the permanent strain rate ($\Delta\varepsilon_{ap,p}$), which reflects the variation of micromechanical mechanism [17, 18]. Werkmeister et al. [22] defined the turning point on the permanent axial strain-load cycle number logarithmic curve as the interface between two stages, and the load number at the boundary point was defined as the number of critical cycles N_0. The specific value method of N_0 is shown in Figure 9 where the strain curves in the two stages are linearly fitted to obtain the fitting curves (1) and (2). The number of loads corresponding to the intersection point "A" of the two fitting lines was N_0. Based on the determination method of N_0, the completion cycle numbers of the compaction stage are all estimated as 100.

To describe the development law of $\Delta\varepsilon_{ap}$ of GRS clearly, a logarithmic processing of vibration times was carried out, and the developments of $\Delta\varepsilon_{ap}$ were plotted against the increase of D-W cycles in Figure 10. $\Delta\varepsilon_{ap,x,y}$ was used to describe $\Delta\varepsilon_{ap}$ of different samples, where x represents the degree of fine particle contents and y represents the numbers of D-W cycles. The following conclusions can be drawn from these experimental results:

(1) The D-W cycles have a significant influence on $\Delta\varepsilon_{ap}$, and with the number of D-W cycles increasing, $\Delta\varepsilon_{ap}$ at the end of load process first decreases and then keeps growing. In Figure 10(a), when $N = 10000$, $\Delta\varepsilon_{ap,K0,0}$ is 1.03%, and it continues to reduce with the increase of D-W cycles until $\Delta\varepsilon_{ap,K0,3}$ keeps the lowest level of 0.61%. Then it increases consistently and ultimately $\Delta\varepsilon_{ap,K0,7}$ reaches 1.61%. Besides, the influence of D-W cycles is mainly reflected in the compression stage. In the compaction stage ($0 \le N \le 100$), the difference between the increase of $\Delta\varepsilon_{ap,K0,0}$ and the increase of $\Delta\varepsilon_{ap,K0,7}$ is only 0.08% (Figure 10(a)). However, in the compression stage ($100 \le N \le 10000$), this difference has already grown to 0.58%, more than seven times that of the compaction stage

(2) The fine particle contents of GRS also influence $\Delta\varepsilon_{ap}$. In Figure 10(a), $\Delta\varepsilon_{ap,K0,0}$ ($N = 10000$) is 1.03%, while $\Delta\varepsilon_{ap,K10,0}$ is 1.52% and $\Delta\varepsilon_{ap,K20,0}$ is 1.71% (in Figures 10(b) and 10(c)). At last, the final $\Delta\varepsilon_{ap,K30,0}$ increases to 2.36% (Figure 10(d)). Therefore, $\Delta\varepsilon_{ap}$ increases with the growth of the fine particles content in the soil sample

4. Permanent Axial Strain of GRS

4.1. Influence of D-W Cycles on the Permanent Axial Strain. As mentioned above, the influence of D-W cycles is mainly reflected in the compression stage with the loading cycles ranging from $N = 100$ to $N = 10000$. The relationship between $\Delta\varepsilon_{ap}$ and the number of D-W cycles in the compression stage is provided in Figure 11. It can be easily found that the influence of D-W cycles on $\Delta\varepsilon_{ap}$ has a certain law. The $\Delta\varepsilon_{ap}$ of the GRS decreases with the increase of D-W cycles in the early stage (0~3times), reflecting the strain hardening and the resistance to deformation increases. However, after 3 D-W cycles (4~7times), $\Delta\varepsilon_{ap}$ of the GRS increases, which exhibits strain softening and resistance to deformation decreases. It indicates that the D-W cycles eventually make the structure of the GRS looser and lead to the increase of $\Delta\varepsilon_{ap}$.

Figure 12 shows the relationship between $\Delta\varepsilon_{ap,p}$ and $\Delta\varepsilon_{ap}$ of GRS in the compression stage. (1) When the number of D-W cycles is relatively small (0~3times), the $\Delta\varepsilon_{ap,p}$ becomes steeper and the permanent strain growth curve gradually slows down, which indicates that the D-W cycles in the early stage make the soil sample more compacted. (2) With the increase of D-W cycles (4~7times), the downtrend of $\Delta\varepsilon_{ap,p}$ becomes relatively moderate, which is manifested by the increase of the abscess span of the strain curve. This means that the D-W cycles increase the length of the compression stage, and the proportion of axial strain in the compression

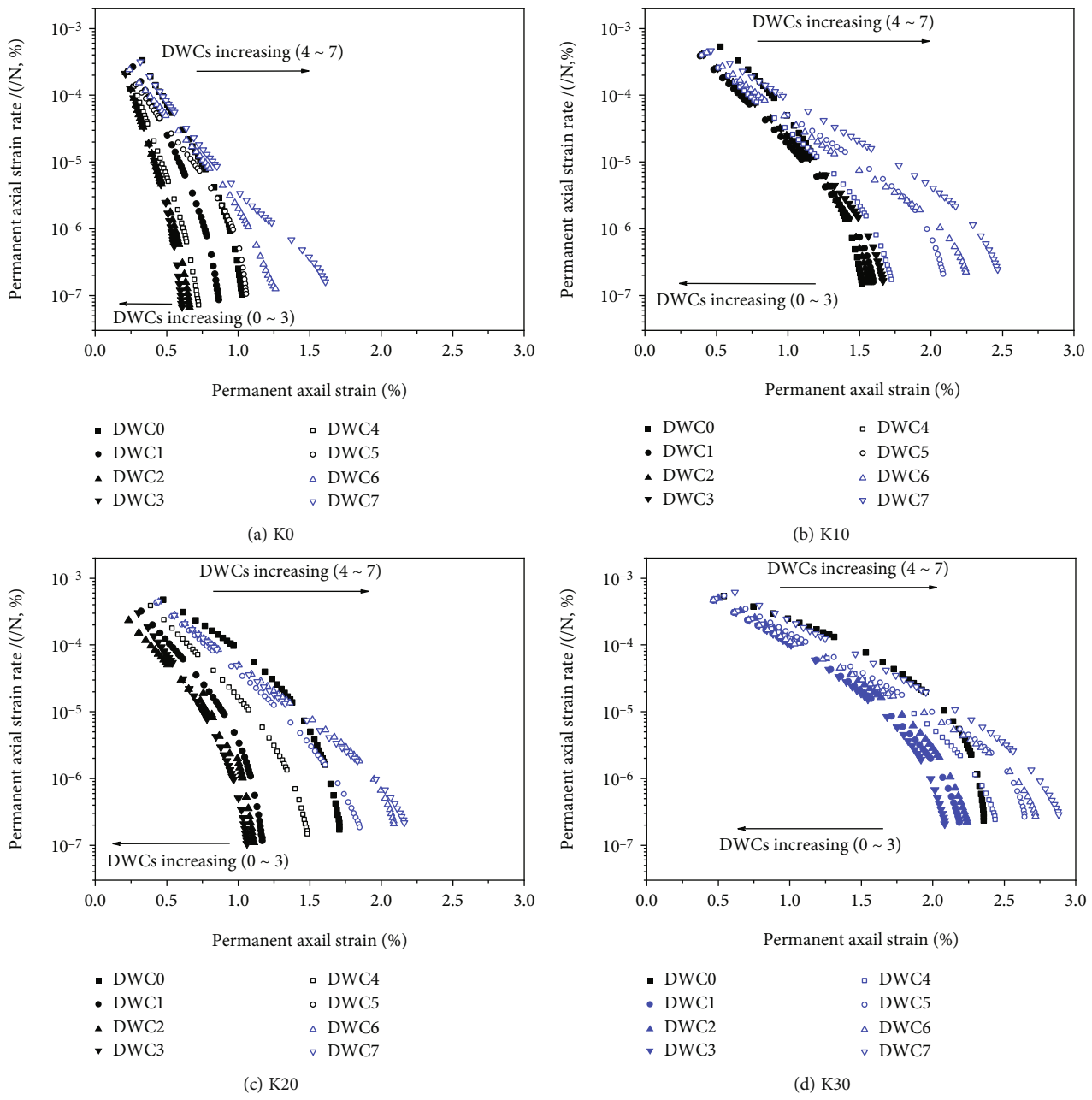

Figure 12: Permanent axial strain rate of GRS under D-W cycles in the compression stage (black points: plastic shakedown; blue points: plastic creep).

stage becomes larger, so that the structure of soil becomes looser.

The coarse particle breakage and compaction under dynamic load are the main factors for the development of $\Delta\varepsilon_{ap}$. Figure 13(a) shows the microstructure of sample without D-W cycles, consisting of fine particles, coarse particles, clay minerals, pore water, and initial cracks. In the early stage of D-W cycles (1~3times, Figure 13(b)), the surface fine particles are lost, and the internal fine particles have different degrees of agglomeration effect during the drying process. Thus, the proportion of coarse particles and the soil's resistance to deformation become larger due to the interlock and friction of coarse particles. However, as the number of D-W cycles goes beyond 3 times (4~7times, Figure 13(c)), for the weak cementation caused by loss of fine particles, coarse particles aggregated by fine particles easily break down into fine particles under dynamic load. Then, inevitably, the soil samples have inner structural defects, as shown by increased cracks and apertures, and the pores are gradually compressed and filled under dynamic load, resulting in a significant increase in the $\Delta\varepsilon_{ap}$ after 3 D-W cycles.

4.2. Influence of Fine Particle Contents on the Permanent Axial Strain. In order to illustrate the influence of internal

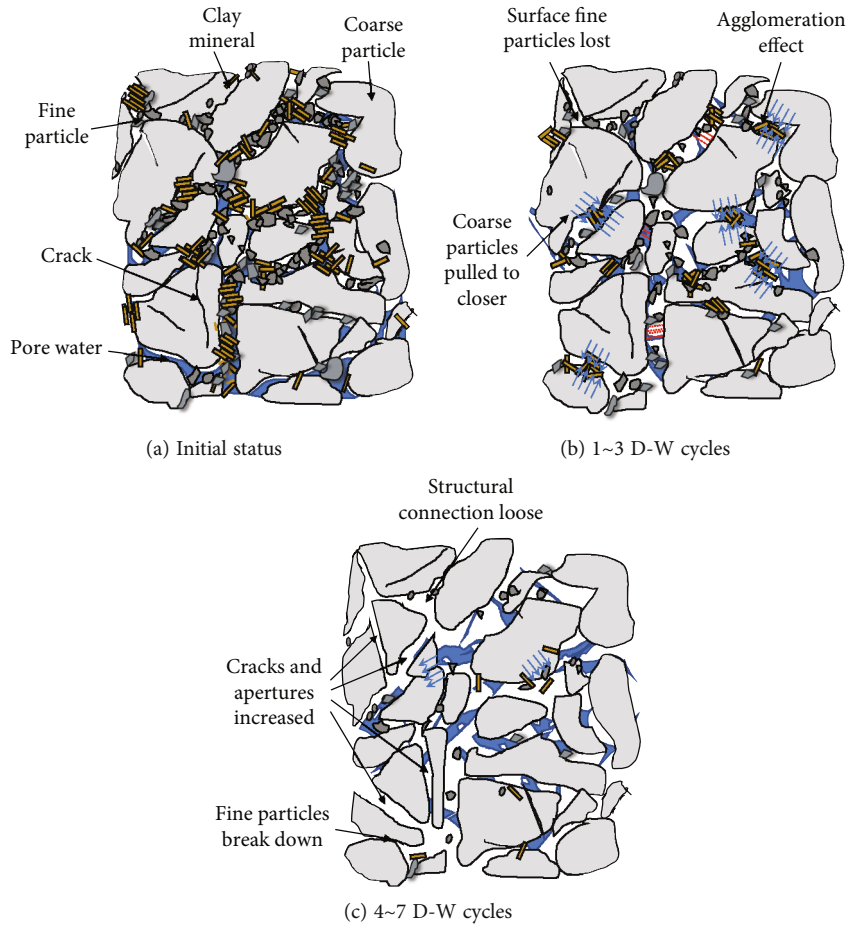

Figure 13: Microstructure changes of GRS with D-W cycles under dynamic loading.

structural components of GRS on $\Delta\varepsilon_{ap}$ under D-W cycles, Figure 14 lists $\Delta\varepsilon_{ap}$ of GRS with respect to fine particle contents after 0, 3, 5, and 7 D-W cycles. The main results can be summarized as follows: (1) in Figure 14(a), without D-W cycles, both $\Delta\varepsilon_{ap}$ and $\Delta\varepsilon_{ap,p}$ increases with the increase of fine particle contents. (2) When the number of D-W cycles increases (Figures 14(b)–14(d)), $\Delta\varepsilon_{ap,K10}$ reaches a higher level than $\Delta\varepsilon_{ap,K20}$. This is due to the fact that with the increase of D-W cycles, only $\Delta\varepsilon_{ap,K10}$ continues to grow, but $\Delta\varepsilon_{ap}$ of other fine particle contents after 3 D-W cycles have an obvious decline compared with 0 D-W cycles soil samples.

Due to the difference between K10 and others, the strain increment change of soil samples, denoted by $\Delta\varepsilon_{ap}$, is depicted in Figure 15, where different fine particle contents in the compaction and compression stages under D-W cycles are considered. The $\Delta\varepsilon_{ap}$ of GRS decreases first and then increases with the D-W cycles in two stages, but it shows different results in the compaction stage for different fine particle contents. In Figure 15(a), $\Delta\varepsilon_{ap,K10}$ is reduced by only 0.03% during the 0~3 D-W cycles, while $\Delta\varepsilon_{ap,K20}$ is reduced by more than 0.59%. On the contrary, in 5~7 D-W cycles, $\Delta\varepsilon_{ap,K10}$ increased by more than 0.18%, while $\Delta\varepsilon_{ap,K20}$ only increased by 0.08%. In the compression stage (Figure 15(b)), the $\Delta\varepsilon_{ap}$ of samples with different fine particle contents change uniformly, which indicates that fine particle contents have less effect on $\Delta\varepsilon_{ap}$ of GRS at this stage.

In the first stage, $\Delta\varepsilon_{ap,K10}$ mainly shows a basically gradual increase in 7 D-W cycles, while $\Delta\varepsilon_{ap}$ of other groups first decreases and then increases. It can be inferred that the effect of particle composition on $\Delta\varepsilon_{ap}$ of GRS is mainly reflected in the compaction stage. With an increase of the content of fine particles in the soil sample, the influence of fine particles on soil deformation can be divided into lubrication, densification, and suffocation (as shown in Figure 16). (1) When the content of fine particles is small, the fine particles act as lubrication on the surface of the coarse particles, and the sliding friction between the coarse particles becomes rolling friction, the deformation resistance between the coarse particles decreases, and the $\Delta\varepsilon_{ap}$ increases. (2) When the content of fine particles increases, the fine particles fill the intergranular pores, and then the compaction resistance of coarse particles increases and the $\Delta\varepsilon_{ap}$ decreases. As the

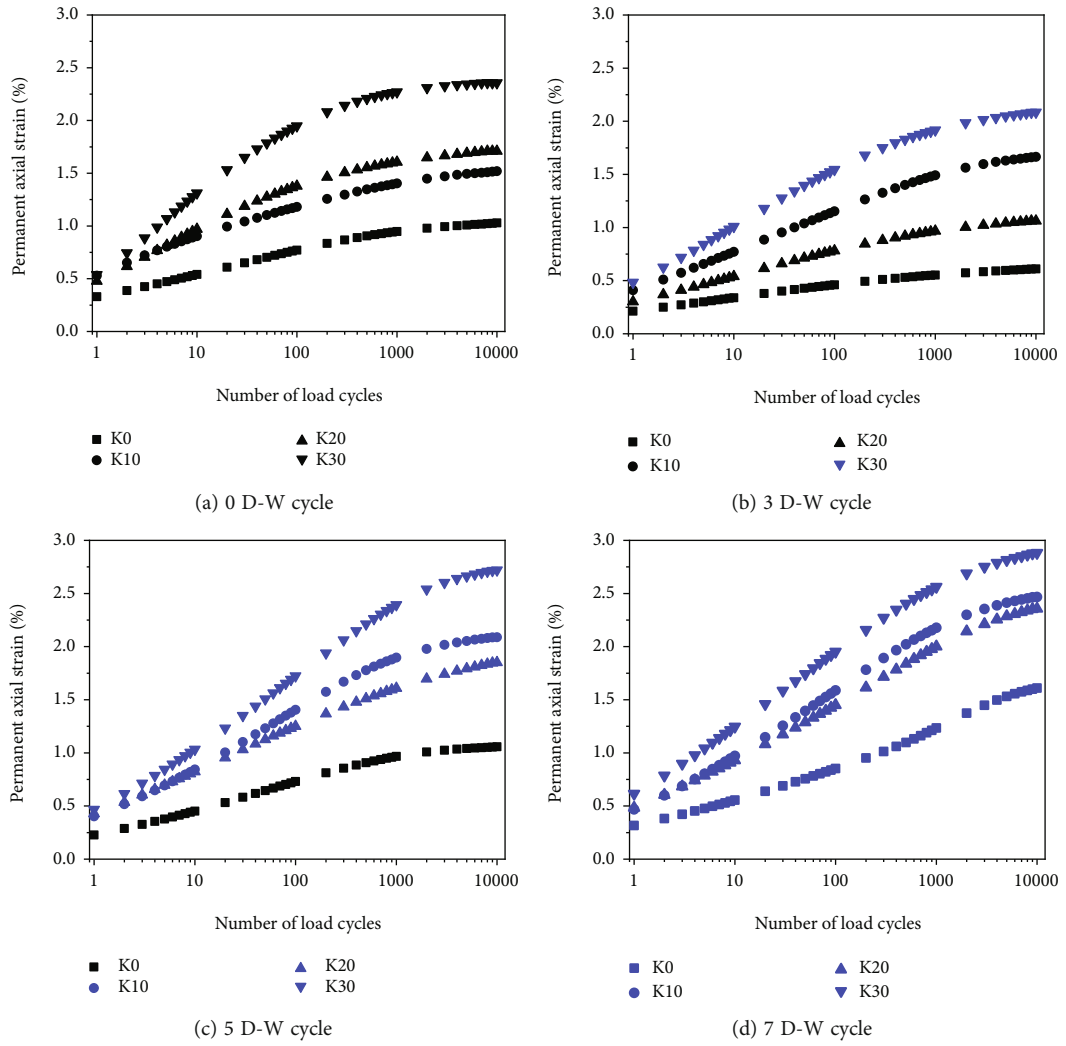

Figure 14: Permanent axial strain of GRS with different fine particle contents. (black point: plastic shakedown; blue point: plastic creep).

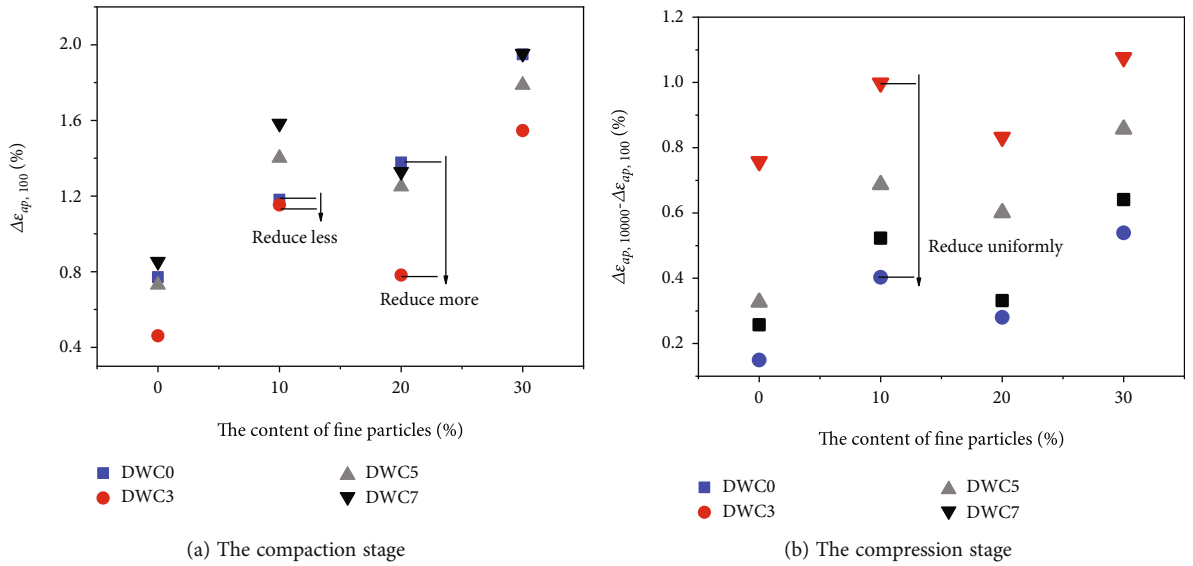

Figure 15: Comparison of permanent axial strain in two stages of GRS.

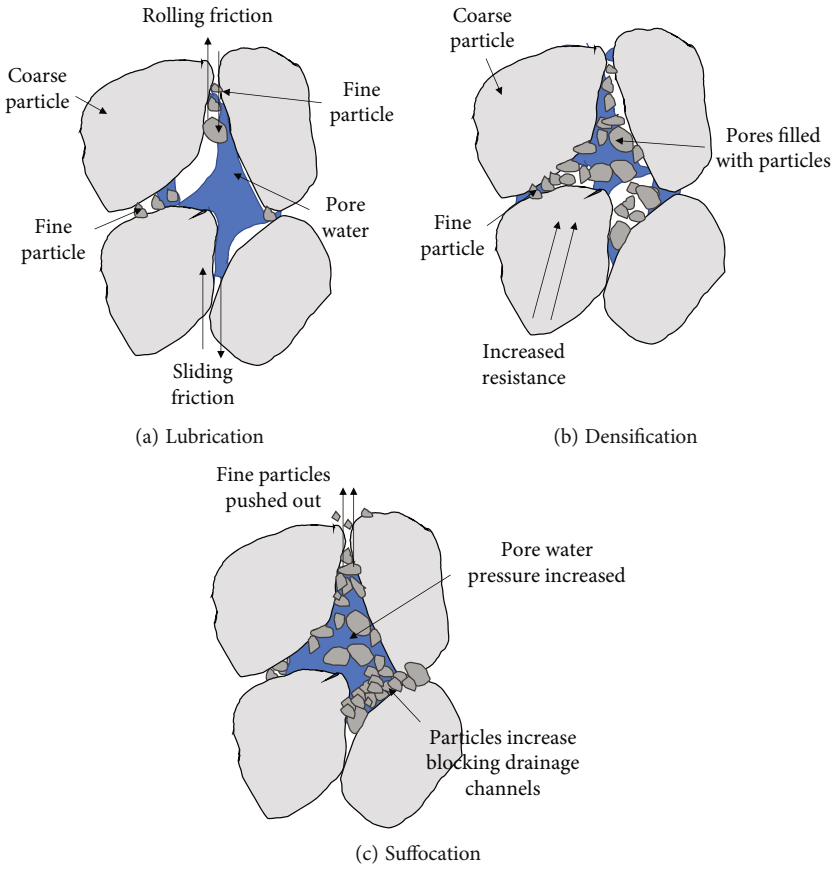

Figure 16: Effect of fine particles on permanent axial strain.

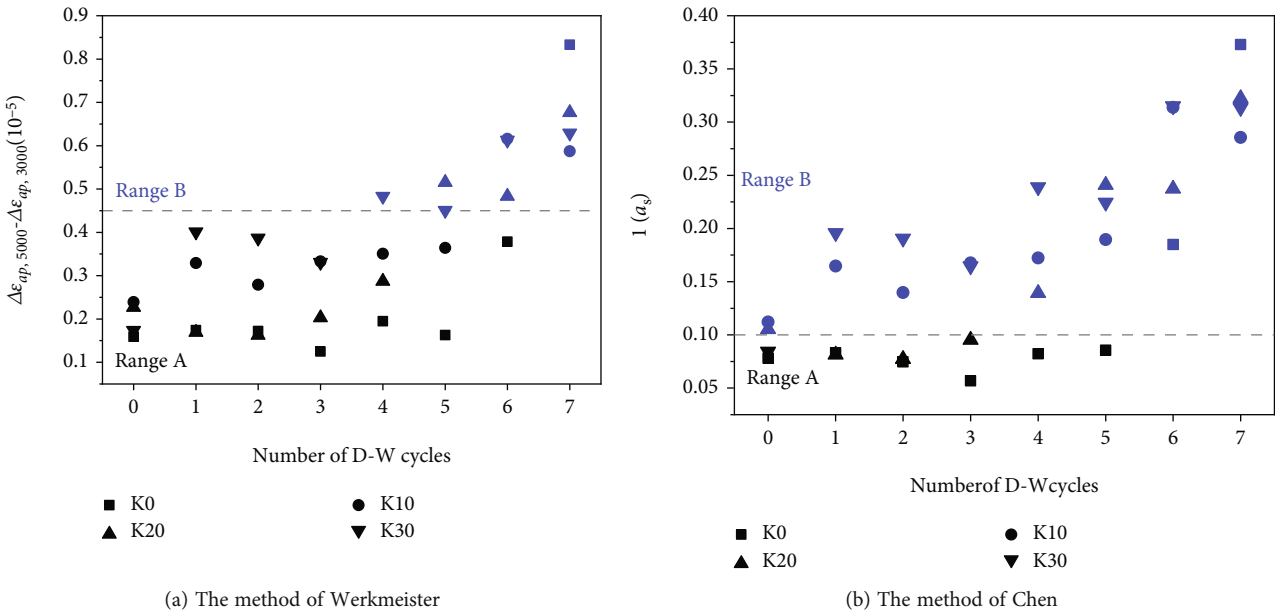

Figure 17: Classification of permanent axial strain of GRS under D-W cycles.

content of fine particles further increases, the fine particles in the pores block the drainage channels of the soil. As a result, the superstatic pore water pressure accumulates, resulting in the suffocation of fine particles. (3) When the pore water pressure accumulates to the limit, the fine particles are pushed out and the $\Delta\varepsilon_{ap}$ increases.

Table 3: The grading results of GRS according to various criteria.

Group	D-W cycles	$\Delta\varepsilon_{ap,5000} - \Delta\varepsilon_{ap,3000}$	$1/a_s$	Werkmeister's criterion [22]	Chen's criterion [18]	Present criterion
K0	0	1.59E-05	0.078	A	A	A
	1	1.74E-05	0.083	A	A	A
	2	1.72E-05	0.075	A	A	A
	3	1.25E-05	0.057	A	A	A
	4	1.95E-05	0.082	A	A	A
	5	1.63E-05	0.086	A	A	A
	6	3.78E-05	0.185	A	B	B
	7	8.33E-05	0.373	B	B	B
K10	0	2.39E-05	0.112	A	B	A
	1	3.29E-05	0.165	A	B	A
	2	2.79E-05	0.140	A	B	A
	3	3.33E-05	0.168	A	B	A
	4	3.50E-05	0.172	A	B	B
	5	3.64E-05	0.190	A	B	B
	6	6.16E-05	0.314	B	B	B
	7	5.87E-05	0.286	B	B	B
K20	0	2.27E-05	0.105	A	B	A
	1	1.69E-05	0.081	A	A	A
	2	1.62E-05	0.077	A	A	A
	3	2.03E-05	0.095	A	A	A
	4	2.87E-05	0.139	A	B	A
	5	5.15E-05	0.241	B	B	B
	6	5.83E-05	0.237	B	B	B
	7	6.77E-05	0.322	B	B	B
K30	0	1.74E-05	0.085	A	A	A
	1	4.01E-05	0.196	A	B	B
	2	3.87E-05	0.191	A	B	B
	3	3.31E-05	0.165	A	B	B
	4	4.83E-05	0.239	B	B	B
	5	5.27E-05	0.225	B	B	B
	6	6.13E-05	0.315	B	B	B
	7	6.29E-05	0.313	B	B	B

5. A New Criterion for Characterization of Shakedown Ranges

For further investigation of the dynamic properties of GRS, Werkmeister et al. divided the definition scope of different deformation types according to the following empirical criteria [22]:

Range A: plastic shakedown.

$$\Delta\varepsilon_{ap,5000} - \Delta\varepsilon_{ap,3000} \leq 4.5 \times 10^{-5}. \quad (1)$$

Range B: plastic creep.

$$4.5 \times 10^{-5} < \Delta\varepsilon_{ap,5000} - \Delta\varepsilon_{ap,3000} \leq 4.0 \times 10^{-4}. \quad (2)$$

Range C: incremental damage.

$$\Delta\varepsilon_{\mathrm{ap},5000} - \Delta\varepsilon_{\mathrm{ap},3000} > 4.0 \times 10^{-4}, \quad (3)$$

where $\Delta\varepsilon_{ap,5000}$ and $\Delta\varepsilon_{ap,3000}$ represent the permanent axial strains corresponding to 5000 and 3000 loading cycles.

At the same time, Chen et al. [18] redefined the permanent axial strain that evolves with the number of loads according to the development rate of plastic strain in the second stage. This specific definition is given as follows:

Range A: plastic shakedown.

$$\frac{1}{a_s} \leq 0.1. \quad (4)$$

Table 4: Survey of permanent axial strain fitting methods.

Fitting models	References	Advantages	Disadvantages
$\varepsilon_{ap} = a \log(N) + b$	Barksdale [32]	Few parameters and simple model form	(1) Models: poor fit accuracy at the later stage (the strain tends to be stable, but the fitting value is still rising) (2) Parameters: no physical meaning (3) Ignore the effects of stress history and environmental change
$\varepsilon_{ap} = aN^b$	Monismith et al. [33]		
$\varepsilon_{ap} = a(\sigma_d/\sigma_s)^m N^b$	Li and Selig [34]		
$\varepsilon_{ap} = N^c/(a + bN^c)$	Zhang et al. [35]		
$\varepsilon_{l,p}(N) = \varepsilon^0_{l,p}(100) + \varepsilon^*_{l,p}(N)$ $\varepsilon^0_{l,p} = a_1(N/100)^{b_1}$ $\varepsilon^*_{l,p} = a_2\left(1 - (N/100)^{-b_2}\right)$	Paute et al. [36] and Nie et al. [27]	Two-stage fitting model High accuracy	(1) Difficult to determine the boundary of different strain stages (2) Ignore the effect of stress history
$\varepsilon_{ap} = a\left(q_d/q_f\right)^m \left(1 + \left(q_s/q_f\right)\right)^n N^b$	Chai and Miura [37]	Considering the dynamic stress level	(1) Models: complex form (2) Parameters: difficult to determine
$\varepsilon_{ap} = \varepsilon^0\left(1 - (N/100)^{-B}\right)(L_{\max}/P_\alpha)^n \bullet (m + (s/P_{\max}) - (q_{\max}/P_{\max}))^{-1}$	Gidel et al. [38]		

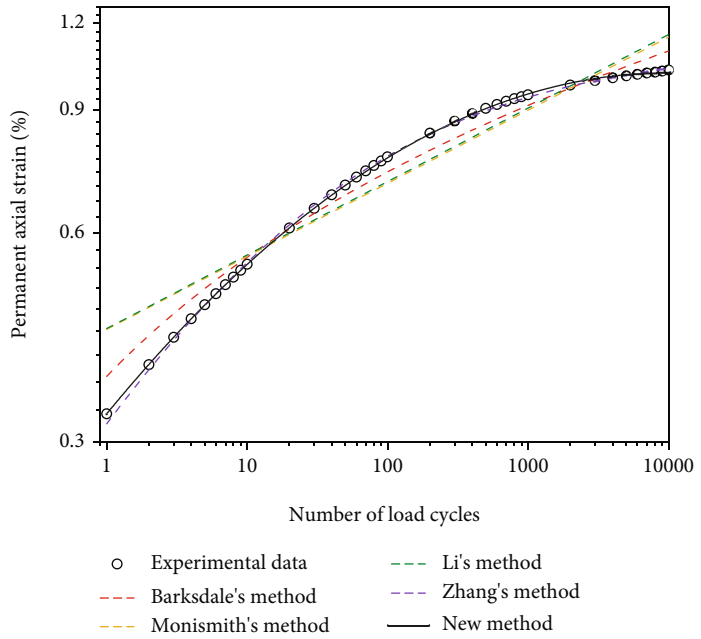

Figure 18: Permanent axial strain fitting (K0 Group).

Range B: plastic creep.

$$0.1 < \frac{1}{a_s} \leq 0.434. \tag{5}$$

Range C: incremental damage.

$$\frac{1}{a_s} > 0.434, \tag{6}$$

where $1/a_s$ is defined as "representative permanent axial strain rate."

The type of permanent axial strain development of GRS is classified in Figure 17. This result illustrates that the type changes from plastic shakedown to plastic creep with an increase in the number of D-W cycles. But it is noted that, based on the two different criteria proposed by Werkmeister and Chen, strain types of GRS permanent strain development under D-W cycles vary between the plastic stability (Range A) and the plastic creep (Range B), and more plastic creep (Range

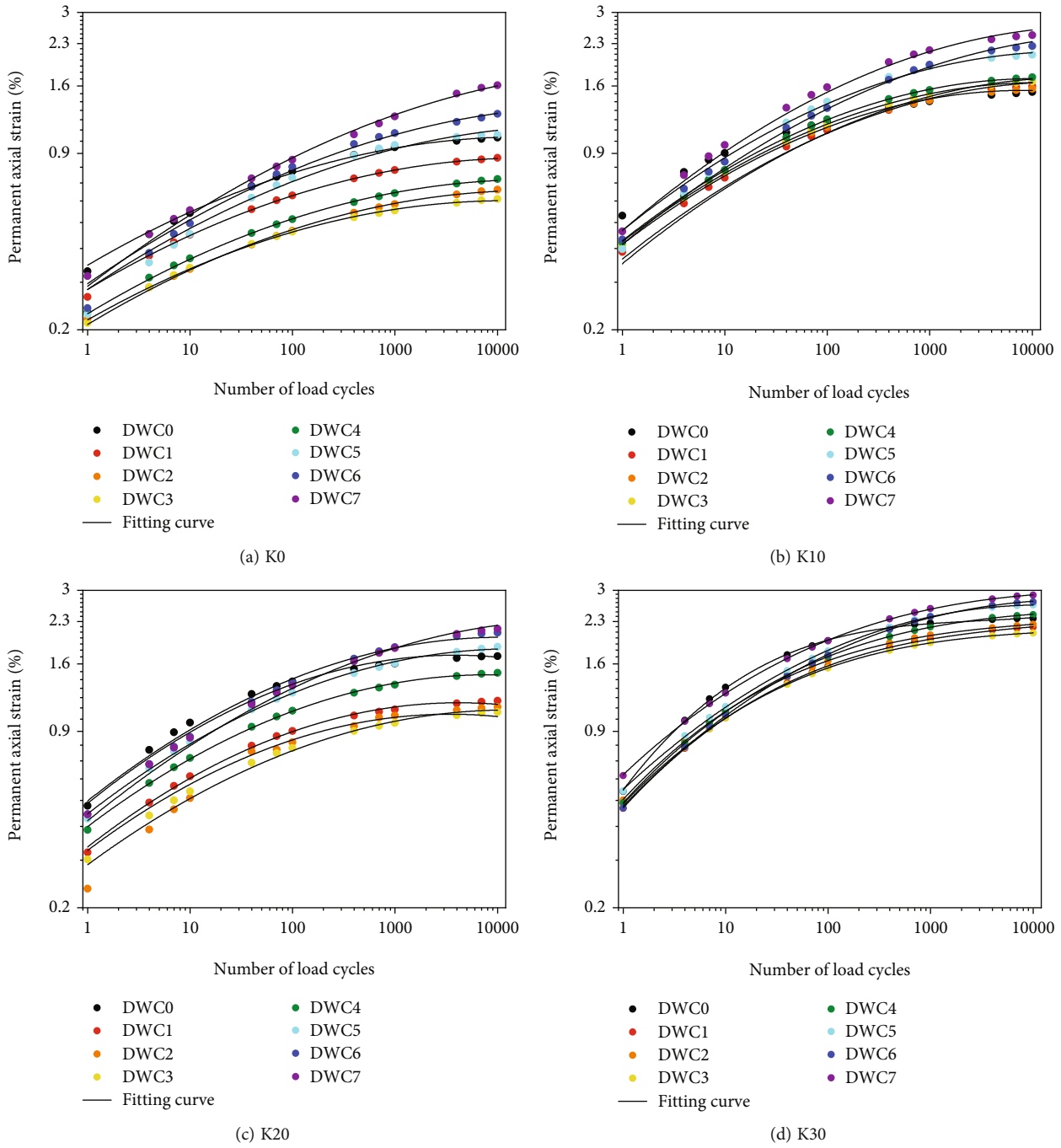

Figure 19: Permanent axial strain fitting of GRS.

B) develops according to Chen's definition. The occurrences of these differences are due to that, Werkmeister's method is mainly based on the amount of $\Delta\varepsilon_{ap}$, while Chen's method basically refers to the strain rate ($\Delta\varepsilon_{ap,p}$).

It is noted that the above methods cannot well calculate the exact interfaces between these two ranges of GRS strain types considered herein. Since GRS is widely used in the railway or highway subgrade, both the amount and the rate of permanent axial strain should be accurately evaluated to meet the subgrade deformation requirements. Therefore, according to the permanent axial strain development laws of GRS, a new criterion considering both strain and strain rate of permanent axial strain is defined as follows:

Range A: plastic shakedown.

The amount of permanent axial strain meets the requirements as:

$$\Delta\varepsilon_{ap,5000} - \Delta\varepsilon_{ap,3000} \le 4.5 \times 10^{-5}. \quad (7)$$

Table 5: Fitting results.

Group	D-W cycles	a	b	c	R^2	Group	D-W cycles	a	b	c	R^2
K0	0	-0.026	0.256	-0.552	0.9441	K20	0	-0.043	0.306	-0.312	0.9859
	1	-0.029	0.239	-0.591	0.9995		1	-0.041	0.295	-0.474	0.9974
	2	-0.022	0.223	-0.633	0.9891		2	-0.04	0.286	-0.558	0.9956
	3	-0.026	0.216	-0.663	0.9992		3	-0.034	0.279	-0.507	0.9992
	4	-0.024	0.218	-0.629	0.9999		4	-0.037	0.287	-0.398	0.9992
	5	-0.024	0.233	-0.546	0.9848		5	-0.035	0.294	-0.351	0.9988
	6	-0.023	0.245	-0.507	0.9929		6	-0.037	0.301	-0.346	0.9999
	7	-0.022	0.255	-0.472	0.9934		7	-0.032	0.31	-0.34	0.9999
K10	0	-0.036	0.314	-0.454	0.9662	K30	0	-0.046	0.349	-0.257	0.9441
	1	-0.035	0.303	-0.437	0.9923		1	-0.046	0.34	-0.258	0.9975
	2	-0.037	0.291	-0.383	0.9986		2	-0.045	0.333	-0.251	0.9972
	3	-0.035	0.288	-0.372	0.9997		3	-0.045	0.328	-0.242	0.9976
	4	-0.037	0.298	-0.369	0.9998		4	-0.046	0.332	-0.234	0.9855
	5	-0.035	0.305	-0.331	0.9962		5	-0.043	0.342	-0.257	0.9999
	6	-0.032	0.314	-0.328	0.9962		6	-0.045	0.364	-0.307	0.9997
	7	-0.035	0.327	-0.332	0.9921		7	-0.04	0.381	-0.37	0.9868

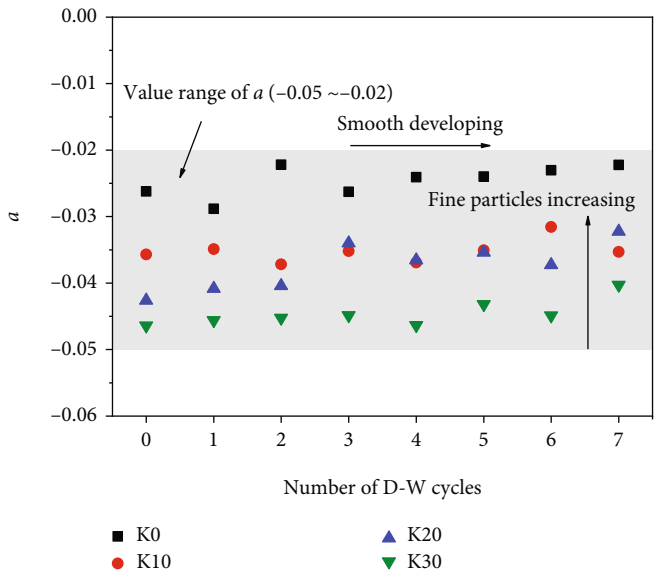

Figure 20: Fitting parameter "a" versus D-W cycles number.

And the permanent axial strain rate is satisfied:

$$\frac{1}{a_s} \leq 0.17. \tag{8}$$

Range B: plastic creep.

If the strain variable and the strain rate can meet, respectively, as

$$4.5 \times 10^{-5} < \Delta\varepsilon_{ap,5000} - \Delta\varepsilon_{ap,3000} \leq 4.0 \times 10^{-4}, \frac{1}{a_s} \leq 0.434. \tag{9}$$

Or the strain variable and the strain rate can meet the following requirements as:

$$\Delta\varepsilon_{ap,5000} - \Delta\varepsilon_{ap,3000} \leq 4.0 \times 10^{-4}, 0.17 < \frac{1}{a_s} \leq 0.434. \tag{10}$$

Range C: incremental damage.

The amount of permanent axial strain meets the requirements as

$$\Delta\varepsilon_{ap,5000} - \Delta\varepsilon_{ap,3000} > 4.0 \times 10^{-4}. \tag{11}$$

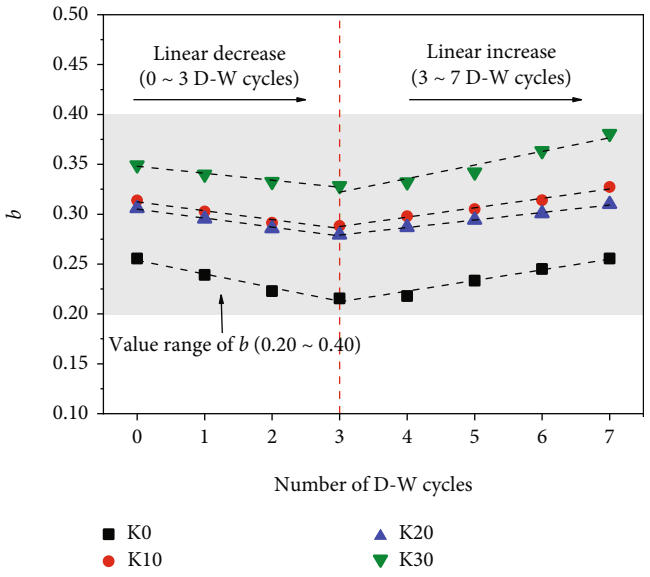

Figure 21: Fitting parameter "b" versus D-W cycles number.

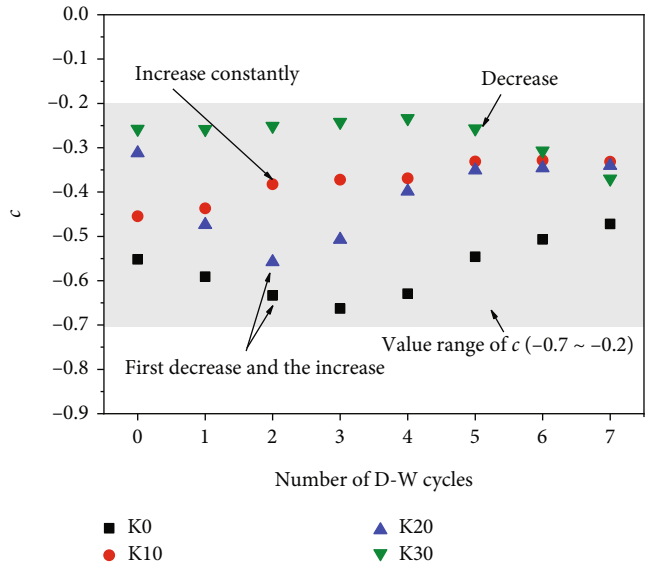

Figure 22: Fitting parameter "c" versus D-W cycles number.

Or the rate of permanent axial strain is satisfied:

$$\frac{1}{a_s} > 0.434. \tag{12}$$

Table 3 lists the grading results of GRS according to Werkmeister's criterion, Chen's criterion, and the present new criterion.

The types of K10 and K20 groups in the new method are obviously different from the two methods of Werkmeister and Chen, but it can better reflect the influence of D-W cycles and fine particle contents. In Figure 12, the permanent axial strain type shifts from plastic shakedown (black point) to plastic creep (blue point) with the increasing times of D-W cycles,

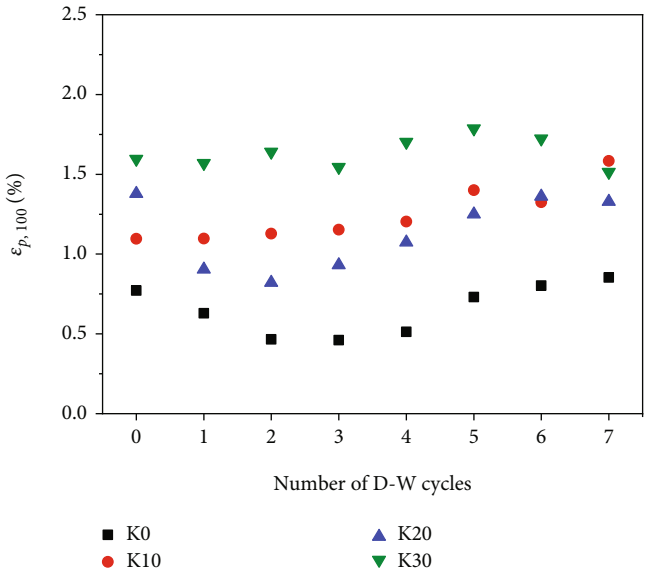

Figure 23: Relationship between permanent axial strain and D-W cycles number in the compaction stage.

but the higher the fine particle contents in the soil sample, the faster transformation rate. It can be seen that K0 group shifts from plastic shakedown to plastic creep after 7 D-W cycles (Figure 12(d)) while the group of K30 needs only 4 D-W cycles (Figure 12(b)). It means that the soil with lower fine particle contents can better adapt to the external actions of both loading cycles and D-W cycles. Besides, it can also be found from Figure 14 that the plastic creep group (blue point) increases with the growth of fine particle contents.

6. Model Fitting for Permanent Strain Prediction

6.1. Fitting Function. Commonly, there are two main approaches to describe $\Delta\varepsilon_{ap}$: one is to establish a constitutive model to simulate the stress-strain relationship of each loading cycle for obtaining $\Delta\varepsilon_{ap}$ and another one is to fit the relationship between $\Delta\varepsilon_{ap}$ and the loading stage, stress level, water content, and other influencing factors to obtain the empirical formula of $\Delta\varepsilon_{ap}$. Table 4 lists the fitting models for $\Delta\varepsilon_{ap}$ frequently used in the existing literatures.

It is noted that the last three models in Table 4 are not suitable for a large number of parameters and different factors. Then the curve of $\Delta\varepsilon_{ap}$ developing with the number of loading cycles is fitted using the first four models in Table 4. The fitting results are shown in Figure 18 (Group K0 was taken as an example for the fitting curve). It can be observed that the fitting results of simple models are not accurate.

Therefore, in this work, due to the $\Delta\varepsilon_{ap}$ curve of GRS presents a nonlinear relationship in the double logarithmic scale, a quadratic function is used to fit, and the fitting function can be expressed as follows:

$$\log\left(\varepsilon_{ap}\right) = a\log^2(N) + b\log(N) + c, \tag{13}$$

where ε_{ap} represents the permanent axial strain; N represents the number of loading cycles; a, b, and c are fitting parameters. The fitting parameters and results are shown in Figure 19 and Table 5.

6.2. Relationship between Fitting Parameters and Number of D-W Cycles. In the quadratic function, coefficient "a" usually controls the opening size and direction of the function image. Figure 20 shows the relationship between the fitting parameter "a" and D-W cycles number. Main conclusions can be drawn as follows: (1) the D-W cycles have little influence on the parameter "a" which varies from -0.05 to -0.02 with D-W cycles. (2) With the increase of fine particle contents, the absolute value of parameter "a" increases. (3) In the load-strain curve, it reflects the speed of strain rate changes. As shown in Figure 14, with the growth of fine particle contents, the change span of strain rate curve increases. That is, the decay of strain rate slows down. Therefore, the absolute value of parameter "a" increases with the growth of fine particle contents. The physical meaning of parameter "a" indicates the decay rate of strain rate, which is greatly affected by the content of fine particles in GRS.

Figure 21 shows the relationship between the fitting value of parameter "b" and D-W cycles number. It can be found that the variation of parameter "b" with the D-W cycles number is similar to the $\Delta\varepsilon_{ap}$ of GRS in the compression stage: (1) in the first 3 D-W cycles, the value of parameter "b" decreases linearly with the increase of D-W cycles number and reaches its lowest point at the 3rd cycle. (2) After 3 D-W cycles, the value of parameter "b" begins to increase linearly. It can be seen that parameter "b" is related to $\Delta\varepsilon_{ap}$ in the compression stage. Moreover, the first order item in quadratic function determines the symmetry axis position of the function image and corresponds to the range of stable strain growth on the load-strain logarithmic curve. Therefore, the following laws can also be found: (1) the physical meaning of parameter "b" represents the increase of the soil strain during the compression stage of GRS, which decreases first and then increases with the growth of the number of D-W cycles. (2) It is greatly affected by fine particle contents, and the value decreases with the increase of fine particle contents. (3) For GRS, the value of "b" is between 0.2 and 0.4.

The fitting relationship between parameter "c" and the number of D-W cycles is given in Figure 22. It can be seen that the values of "c" of different fine particle contents vary with the D-W cycles: (1) when the fine particle content is very low (K0 group), the parameter "c" decreases first and then increases with the growing of D-W cycles, and the growth rate decreases in the later period. (2) With the increase of fine particle content (K10), the parameter "c" becomes larger as the D-W cycles increase and finally tends to a fixed value. (3) When the fine particle content continues to increase (K20 group), the change of parameter "c" shows a trend of decreasing first and then increasing, and the minimum value of "c" is obtained at the 2nd D-W cycles. (4) When the fine particle content continues to rise (K30 group), the parameter "c" firstly increases and then decreases. In the load-strain logarithmic curve, parameter "c" represents the logarithm value of $\Delta\varepsilon_{ap}$ in the initial stage of load, so it can be noted that it is related to $\Delta\varepsilon_{ap}$ in the compaction stage. Figure 23 shows the variation rule of the early $\Delta\varepsilon_{ap}$ of GRS with different fine particle contents under D-W cycles, which is obviously similar to the variation rule of parameter "c".

7. Conclusions

Based on the dynamic triaxial test of GRS with D-W cycles and varying fine particle contents, the growth law of $\Delta\varepsilon_{ap}$ was investigated from three aspects: strain development, mechanism analysis, and prediction model. The main results were summarized as follows:

(1) In accordance with Werkmeister's method, the permanent strain curve can be divided into two stages: the compaction stage and the compression stage. The influence of D-W cycles on $\Delta\varepsilon_{ap}$ of GRS is mainly embodied in the compression period, and this is because the first 3 D-W cycles make the soil more compact and $\Delta\varepsilon_{ap}$ smaller. After 3 D-W cycles, the soil becomes loose and soft and $\Delta\varepsilon_{ap}$ increases

(2) The influence of fine particle contents on $\Delta\varepsilon_{ap}$ mainly happens in the compaction stage, including lubrication, densification, and asphyxiation. When the content of fine particles is relatively low (K10), the $\Delta\varepsilon_{ap}$ of GRS increases. While the fine particle content is medium (K20), $\Delta\varepsilon_{ap}$ is small. The $\Delta\varepsilon_{ap}$ increases when fine particle content goes high (K30). The effect will change with the increase of D-W cycles number, but the mechanism of this change needs further study

(3) The permanent strains following the criteria of Werkmeister and Chen are quite different. To overcome this issue, a new criterion for $\Delta\varepsilon_{ap}$ of GRS has been proposed, which considers the requirements of the variable and strain rate together and can better simulate the actual situation of roadbed strain. The test data judged by the proposed new criteria show that with the increase of D-W cycles, the permanent strain development type of GRS gradually changes from plastic stabilization to plastic creep, and the transition often occurs after 4~5 D-W cycles

(4) In the log-log coordinate system, the quadratic function can be used to fit the relationship between $\Delta\varepsilon_{ap}$ and the loading cycle number of GRS under D-W cycles. The prediction model parameters represent the strain rate, compression strain, and compaction strain, respectively

Data Availability

The data are available and are explained in this article; readers can access the data supporting the conclusions of this study.

Conflicts of Interest

The authors declare that there is no conflict of interest regarding the publication of this paper.

Acknowledgments

The work in this paper is supported by the National Engineering Laboratory for High-Speed Railway Construction Technology (No. HSR201909) and the Natural Science Foundation of Fujian Province (No. 2021J01010).

References

[1] H. Rahardjo, A. Satyanaga, E. C. Leong, Y. S. Ng, and H. T. C. Pang, "Variability of residual soil properties," *Engineering Geology*, vol. 141-142, pp. 124–140, 2012.

[2] S. M. Dasaka and L. M. Zhang, "Spatial variability of in situ weathered soil," *Géotechnique*, vol. 62, no. 5, pp. 375–384, 2012.

[3] L. W. Kong, H. M. Sayem, and H. Tian, "Influence of drying-wetting cycles on soil-water characteristic curve of undisturbed granite residual soils and microstructure mechanism by nuclear magnetic resonance (NMR) spin-spin relaxation time (T2) relaxometry," *Canadian Geotechnical Journal*, vol. 55, no. 2, pp. 208–216, 2018.

[4] P. Liu, R. P. Chen, and X. Kang, "Effects of drying-wetting cycles on the mechanical behavior of reconstituted granite-residual soils," *Journal of Materials in Civil Engineering*, vol. 32, no. 8, article 04020199, 2020.

[5] X. R. Niu, H. Y. Xie, Y. F. Sun, and Y. P. Yao, "Basic physical properties and mechanical behavior of compacted weathered granite soils," *International Journal of Geomechanics*, vol. 17, no. 10, article 04017082, 2017.

[6] I. M. Lee, S. G. Sung, and G. C. Cho, "Effect of stress state on the unsaturated shear strength of a weathered granite," *Canadian Geotechnical Journal*, vol. 42, no. 2, pp. 624–631, 2005.

[7] Y. Wang, S. X. Zhang, S. Yin, X. Y. Liu, and X. Zhang, "Accumulated plastic strain behavior of granite residual soil under cycle loading," *International Journal of Geomechanics*, vol. 20, no. 11, p. 04020205, 2020.

[8] S. Yin, L. W. Kong, A. W. Yang, and K. Mu, "Indoor experimental study of road performance of granite residual soil for subgrade filling materials," *Rock and Soil Mechanics*, vol. 37, pp. 287–293, 2016.

[9] D. Q. Zhou, H. J. Tan, and Y. M. Xu, "Indoor experimental study for accumulative and wetting deformation of granite residual soil under cyclic loading," *Journal of Central South University: Science and Technology*, vol. 44, no. 4, pp. 1657–1665, 2013.

[10] S. M. Rao and K. Revanasiddappa, "Influence of cyclic wetting drying on collapse behaviour of compacted residual soil," *Geotechnical & Geological Engineering*, vol. 24, no. 3, pp. 725–734, 2006.

[11] M. Muntaha, R. A. Soemitro, and D. D. Warnana, "The static and dynamic characteristic of undisturbed residual soils under drying-wetting cycle's repetition," *Japanese Geotechnical Society Special Publication*, vol. 2, no. 15, pp. 591–594, 2015.

[12] B. Indraratna, N. Tennakoon, S. Nimbalkar, and C. Rujikiatkamjorn, "Behaviour of clay-fouled ballast under drained triaxial testing," *Géotechnique*, vol. 63, no. 5, pp. 410–419, 2013.

[13] H. Rahardjo, K. K. Aung, E. C. Leong, and R. B. Rezaur, "Characteristics of residual soils in Singapore as formed by weathering," *Engineering Geology*, vol. 73, no. 1-2, pp. 157–169, 2004.

[14] R. An, L. W. Kong, C. S. Li, and X. Q. Lu, "Strength attenuation and microstructure damage of granite residual soils under hot and rainy weather," *Chinese Journal of Rock Mechanics and Engineering*, vol. 39, no. 9, pp. 1902–1911, 2020.

[15] T. V. Duong, Y. J. Cui, A. M. Tang et al., "Physical model for studying the migration of fine particles in the railway substructure," *Geotechnical Testing Journal*, vol. 37, no. 5, article 20130145, 2014.

[16] T. V. Duong, Y. J. Cui, A. M. Tang et al., "Investigating the mud pumping and interlayer creation phenomena in railway sub-structure," *Engineering Geology*, vol. 171, pp. 45–58, 2014.

[17] W. B. Chen, W. Q. Feng, J. H. Yin, J. M. Chen, L. Borana, and R. P. Chen, "New model for predicting permanent strain of granular materials in embankment subjected to low cyclic loadings," *Journal of Geotechnical and Geoenvironmental Engineering*, vol. 146, no. 9, article 04020084, 2020.

[18] W. B. Chen, W. Q. Feng, J. H. Yin, L. Borana, and R. P. Chen, "Characterization of permanent axial strain of granular materials subjected to cyclic loading based on shakedown theory," *Construction and Building Materials*, vol. 198, pp. 751–761, 2019.

[19] H. Y. Lei, Y. J. Song, Z. Y. Qi, J. J. Liu, and X. Liu, "Accumulative plastic strain behaviors and microscopic structural characters of artificially freeze-thaw soft clay under dynamic cyclic loading," *Cold Regions Science and Technology*, vol. 168, article 102895, 2019.

[20] M. S. Rahman and S. Erlingsson, "Predicting permanent deformation behaviour of unbound granular materials," *International Journal of Pavement Engineering*, vol. 16, no. 7, pp. 587–601, 2015.

[21] S. Yin, L. W. Kong, and X. W. Zhang, "Experimental study on stiffness characteristics of residual soil at small strain under hot and rainy climate," *Chinese Journal of Geotechnical Engineering*, vol. 39, no. 4, pp. 743–751, 2017.

[22] S. Werkmeister, F. Wellner, and A. R. Dawson, "Permanent deformation behaviour of granular materials," *Road Materials and Pavement Design*, vol. 6, no. 1, pp. 31–51, 2005.

[23] Z. Y. Li, X. W. Cao, and Q. Xie, "Test study of dynamic characteristics of granitic residual soil for highway subgrade," *Rock and Soil Mechanics*, vol. 27, no. 12, pp. 2269–2272, 2006.

[24] L. S. Tang, Z. L. Zhao, H. K. Chen, Y. P. Wu, and C. ZengY, "Dynamic stress accumulation model of granite residual soil under cyclic loading based on small-size creep tests," *Journal of Central South University*, vol. 26, no. 3, pp. 728–742, 2019.

[25] National Railway Administration of the People's Republic of China, *Code for Design of Railway Earth Structure,TB 10001-2016*, Chian Railway Publishing House, Beijing, 2017.

[26] Y. F. Li, R. S. Nie, Z. R. Yue, W. M. Leng, and Y. P. Guo, "Dynamic behaviors of fine-grained subgrade soil under single-stage and multi- stage intermittent cyclic loading: permanent deformation and its prediction model," *Soil Dynamics and Earthquake Engineering*, vol. 142, article 106548, 2021.

[27] R. S. Nie, Y. F. Li, W. M. Leng, H. H. Mei, J. L. Dong, and X. X. Chen, "Deformation characteristics of fine-grained soil under cyclic loading with intermittence," *Acta Geotechnica*, vol. 15, no. 11, pp. 3041–3054, 2020.

[28] X. S. Shi, I. Herle, and W. D. Muir, "A consolidation model for lumpy composite soils in open-pit mining," *Géotechnique*, vol. 68, no. 3, pp. 189–204, 2018.

[29] X. S. Shi and I. Herle, "Numerical simulation of lumpy soils using a hypoplastic model," *Acta Geotechnica*, vol. 12, no. 2, pp. 349–363, 2017.

[30] X. S. Shi and J. D. Zhao, "Practical estimation of compression behavior of clayey/silty sands using equivalent void-ratio concept," *Journal of Geotechnical and Geoenvironmental Engineering*, vol. 146, no. 6, article 04020046, 2020.

[31] H. Xiong, F. Nicot, and Z. Y. Yin, "A three-dimensional micromechanically based model," *International Journal for Numerical and Analytical Methods in Geomechanics*, vol. 41, no. 17, pp. 1669–1686, 2017.

[32] R. D. Barksdale, "Laboratory evaluation of rutting in base course materials," in *Presented at the Third International Conference on the Structural Design of Asphalt Pavements, Grosvenor House, Park Lane*, pp. 161–174, London, England, 1972.

[33] C. L. Monismith, N. Ogawa, and C. R. Freeme, "Permanent deformation characteristics of subgrade soils due to repeated loading," *Transportation Research Record*, vol. 537, pp. 1–17, 1975.

[34] D. Q. Li and E. T. Selig, "Cumulative plastic deformation for fine-grained subgrade soils," *Journal of Geotechnical and Geoenvironmental Engineering*, vol. 122, no. 12, pp. 1006–1013, 1996.

[35] Y. Zhang, L. W. Kong, A. G. Guo, and X. W. Li, "Cumulative plastic strain of saturated soft clay under cyclic loading," *Chinese Journal of Geotechnical Engineering*, vol. 30, no. 6, pp. 1542–1548, 2009.

[36] J. L. Paute, P. Hornych, and J. P. Benaben, "Repeated load triaxial testing of granular materials in the French network of laboratories des Ponts et Chaussées," in *Proceedings of The European Symposium Euroflex*, pp. 53–64, Lisbon, Portugal, 1996.

[37] J. C. Chai and N. Miura, "Traffic-load-induced permanent deformation of road on soft subsoil," *Journal of Geotechnical and Geoenvironmental Engineering*, vol. 128, no. 11, pp. 907–916, 2002.

[38] G. Gidel, P. Hornych, J. J. Chauvin, D. Breysse, and A. Denis, "A new approach for investigating the permanent deformation behaviour of unbound granular material using the repeated loading triaxial apparatus," *Bulletin des Liaison Laboratory Ponts et Chaussées*, vol. 233, pp. 5–21, 2001.